symmetry

MDPI

Article

Design of an Optically Transparent Microwave Absorber Based on Coding Metasurface

Senfeng Lai *, Guiyang Liu, Yanpei Guo and Yang Liu

School of Electronic and Information, Guangdong Polytechnical Normal University, Guangzhou 510665, China
* Correspondence: laisenfeng@gpnu.edu.cn

Abstract: In this paper, a metamaterial absorber with a checkerboard patterned ITO (indium tin oxide) film as the surface is obtained by using flexible and optically transparent wave-absorbing material ITO–PET (polyethylene terephthalate), and a coding arrangement of two basic coding units based on the APS-PSO (Array Pattern Synthesis -Particle Swarm Optimization) algorithm. The surface structure of the absorber consists of ITO rectangular patch structures and ITO circular patch structures (110 Ω/sq). The ITO rectangular patch structures and ITO circular patch structures are symmetrical. The middle layer is made up of two layers of PET and one layer of PMMA, and the bottom surface is covered with a layer of low square resistance ITO film (8 Ω/sq). The experimental results, which are consistent with the simulation results, show that the absorber has superior performance: over 90% absorptance in the 5.06–9.01 GHz band, high transmittance, and a −10 dBsm RCS (radar cross-section) reduction in the 5.3–8.7 GHz band. This design also has polarization insensitivity and angular stability.

Keywords: microwave absorber; coding metasurface; flexible and optically transparent; RCS reduction

check for updates

Citation: Lai, S.; Liu, G.; Guo, Y.; Liu, Y. Design of an Optically Transparent Microwave Absorber Based on Coding Metasurface. *Symmetry* **2022**, *14*, 2217. https://doi.org/10.3390/sym14102217

Academic Editors: Ben-Xin Wang, Han Xiong and Qi Lin

Received: 21 September 2022
Accepted: 19 October 2022
Published: 21 October 2022

1. Introduction

The metamaterial is an engineered periodic structure composed of subwavelength units with extraordinary electromagnetic properties. It is used in a variety of applications in the microwave to the terahertz frequency range [1–8]. Artificially construct metamaterials can exhibit negative refractive indices [9], which can lead to new optical phenomena [10]. The metamaterial microwave absorber is designed by processing and designing the shape, size, and method of combining artificial composite materials for producing efficient absorptance in the very narrow or wide frequency bandwidth. At the moment, metamaterials are used in industrial and military fields [11] such as communication, stealth and mid-infrared and thermal detection devices [12]. Thus, research on metamaterial microwave absorbers is crucial to improve the performance of these applications. In recent years, several microwave absorbers with new properties [13,14] have been proposed, and the perfect microwave loss characteristics can be achieved by designing the basic unit structure of the metamaterials. Since the characteristics of a metamaterial depend primarily on the geometry, they can be used in a specific electromagnetic spectrum. The perfect loss design of metamaterials overcomes the thickness limitation of traditional absorbers, and the limitation of microwave absorptance efficiency. In addition, depending on the substrate and geometries used, the metasurface can be used for high quality switching between reflection and transmission, phase control and significant resonant behavior within the spectral window of interest [15].

Metamaterial absorbers based on resistive films have thin profiles that are easier to build and shape. Representative resistive materials that can be used for wave-absorbing structures are ITO and ATO (antimony tin oxide), with ITO being more frequently chosen due to its relatively high optical transparency [16]. Optical transparency can be a critical requirement in certain application situations, for example, the plane windows or the display screen glass that needs to shield the microwave yet transmit the visible

light, and the radome, which needs to transmit both microwave and visible light. The optically transparent absorbers are more suitable for displays, phones, and glass windows of military vehicles [17,18].

In recent years, RCS reduction technology [19] has become an important research element in electromagnetic stealth topics, which can be divided into two directions: one uses the perfect metamaterial absorber (PMA) proposed by Landy in 2008 [20], which adopts an ultra-thin structure and has a nearly single absorptance rate to achieve high absorptance over a wide frequency band; the other uses the coding metasurface absorber proposed by Tiejun Cui in 2014 [21], which employs various combinations of artificial magnetic conductors to modulate the absorber surface phase, change its scattering field, and achieve diffuse reflection, thereby reducing RCS.

In the field of electromagnetic shielding, new metamaterials and coding techniques have been widely used in the microwave band [22]. The coding metasurface absorber can be applied to the surface of an object to improve its RCS reduction, which is a novel method of modulating microwaves that has great potential in radar stealth, imaging, and broadband communication fields [23,24].

In this paper, we design an absorber using optically transparent absorbing material (ITO) as the coding metasurface. Based on the APS-PSO algorithm, the spatial arrangement of the encoded basic unit is designed by regulating the scattering field of the absorber so that the incident electromagnetic wave is diffusely reflected and the RCS reduction is achieved. It has over 90% absorptance in the 5.06–9.01 GHz band, high transmittance, and a −10 dBsm RCS reduction band from 5.3–8.7 GHz. This design also has polarization insensitivity and angular stability, with promising applications in flat panel displays, low radiation glass, special functional window coatings, etc.

2. Design and Simulation

The structure of a rectangular patch and a circular patch unit is shown in Figure 1. The structure of a rectangular patch unit is shown in Figure 1a, where the top layer of the unit consists of four 13 mm × 13 mm rectangular ITO film patches with a square resistance of 110 Ω/sq. The structure of a circular patch unit is shown in Figure 1b, where the top layer of the unit is made up of four circular ITO film patches with a radius of 3 mm and a square resistance of 110 Ω/sq. The ITO rectangular patch structures and ITO circular patch structures are symmetrical.

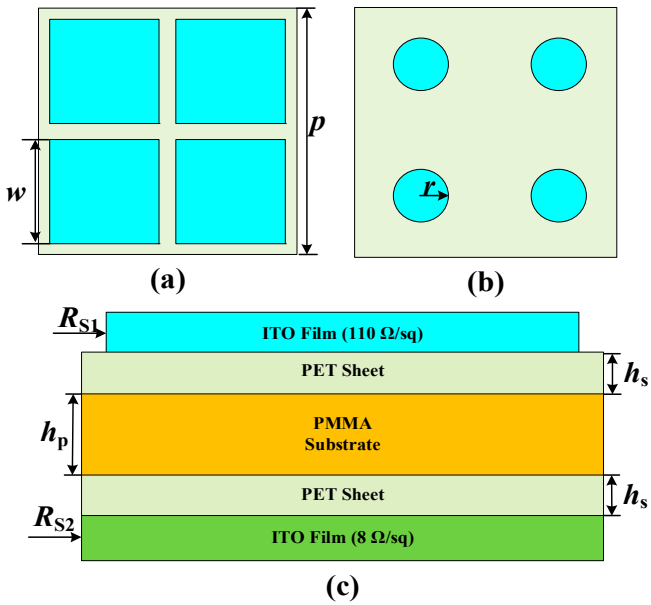

Figure 1. Unit structure. (**a**) Top view of rectangular patch. (**b**) Top view of circular patch. (**c**) Side view of the unit.

As shown in Figure 1c, both rectangular and circular unit structures have a sandwich structure consisting of five layers. The upper surface is made up of a simple patterned ITO thin film resistive patch (R_{s1} = 110 Ω/sq). The ground plane is made of a low-resistance ITO thin film (R_{s2} = 8 Ω/sq), which completely reflects the incident wave and ensures that the microwave cannot pass through the absorber. The ITO films are printed on both the upper surface and the ground plane on two flexible polyethylene terephthalate (PET) sheets (relative permittivity of 3.0, dielectric loss tangent of 0.06, and thickness of h_s). PMMA (relative permittivity of 2.25, dielectric loss tangent of 0.01, thickness of h_p) is in the middle of two PET layers. Therefore, the PMMA layer is the middle layer of the sandwich structure. To ensure the high light transmission of the proposed metamaterial absorber, all materials used in the design have high visible light transmission. In this paper, we use 110 Ω/sq ITO film to form a patterned resistive metasurface to efficiently dissipate the incident energy. The resistance of ITO films can be fine-tuned by precisely controlling the film thickness. The detail of the parameters of the proposed structure, shown in Figure 1, is given in Table 1.

Table 1. The parameters of the unit structure shown in Figure 1.

h_s	h_p	w	p	r	R_{S1}	R_{S2}
0.3 mm	5.6 mm	13 mm	30 mm	3 mm	110 Ω	8 Ω

As the frequency increases, the reflection coefficient phase of the proposed unit structure changes from +180° to −180° (Figure 2a). At the resonant frequency of 3.4 GHz, the reflection phase of the circular patch reaches 0° and the reflection coefficient at the resonant frequency is −0.57 dB (Figure 2b). At the resonant frequency of 3.22 GHz, the reflection phase of the rectangular patch reaches 0° and the reflection coefficient at the resonant frequency is −8.82 dB, which is attributed to the dielectric and radiation losses. Because of the 180° reflection phase difference between them, they can be used as "0" and "1" in the coding sequence to increase the frequency bandwidth of the RCS reduction.

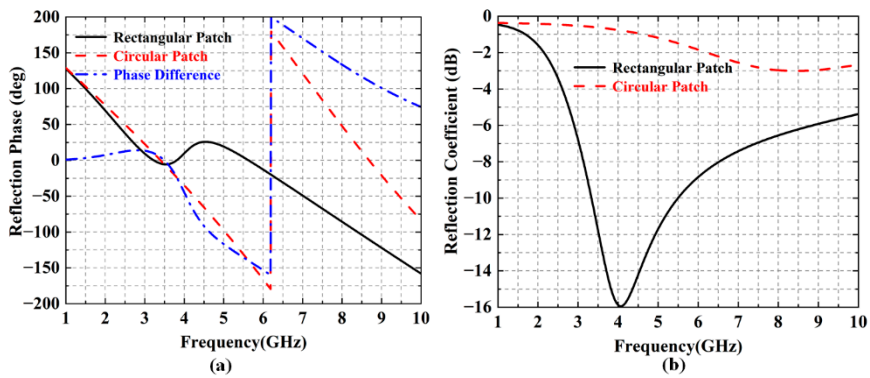

Figure 2. (**a**) Phase difference of absorber unit as a function of frequency. (**b**) Reflection coefficient of absorber unit as a function of frequency.

Different coding sequences yield different electromagnetic properties, so the optimization of the coding sequences is particularly important to enhance the performance of the absorber and the RCS reduction. Based on the particle swarm algorithm, the spatial arrangement of the encoded basic unit is designed by regulating the scattering field of the absorber so that the incident electromagnetic wave is diffusely reflected and the RCS reduction is achieved. Combining the integrated algorithm of PSO and APS, the phase of the coding metasurface can be optimized quickly to obtain the best performance of the coding metasurface absorber. The PSO module evaluates the fitness in each iteration, keeps track of the particle velocities and population positions, and then shares the information with the APS module using the APS-PSO algorithm to encode the above two basic encoding units in an arrangement. The algorithm is implemented using Matlab, and the population

particle position, i.e., the coding sequence is optimized and considered as a random matrix (containing only 0 and 1), as is the particle velocity.

The metasurface cell structure has an initial value of 0 or 1 corresponding to 0 or π. The curve of the fitness function obtained by numerical optimization using Matlab is shown in Figure 3. It can be seen that the curve decreases rapidly in the initial stage and then stabilizes, indicating that the APS-PSO algorithm has high efficiency.

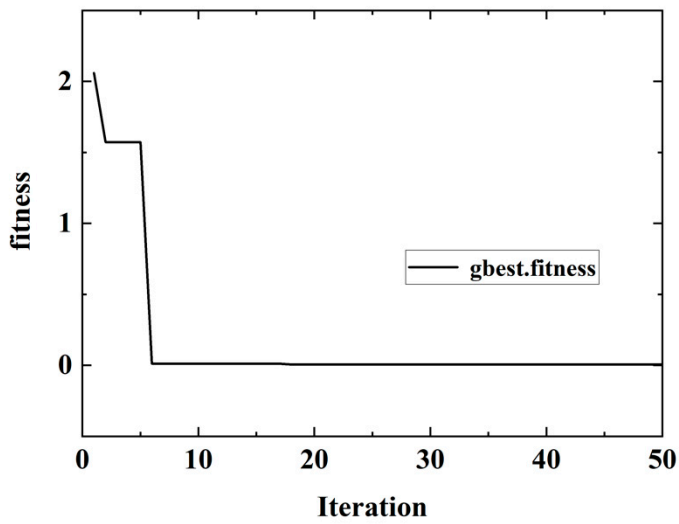

Figure 3. Adaptive evolution curve.

The APS module calculates the RCS reduction with the current phase arrangement, and then calculates the fitness function value and returns it to the PSO module. After several iterations, the phase arrangement of the coding metasurface with the maximum RCS reduction is obtained. The structure of the coding sequence absorber is shown in Figure 4.

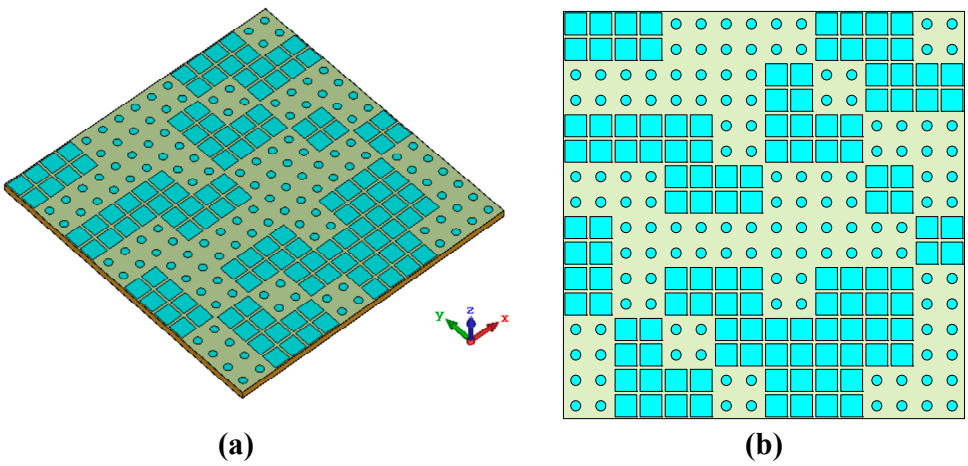

Figure 4. (**a**) Absorber structure. (**b**) Top view of the absorber.

The simulation of the optically transparent absorber is performed by finite integration technique using the CST MWS software. Floquet ports with normal incident plane transverse electric (TE) waves and transverse magnetic (TM) waves were set in the z-direction for excitation. Periodic boundary conditions (PBCs) along the x and y directions were used to simulate the infinite periodic element, and frequency-dependent complex S parameters can be simulated by the frequency domain solver.

To maximize the absorptance $A(\omega)$, we need to minimize the reflectance $R(\omega)$ and transmittance $T(\omega)$. The absorptance of a microwave absorber is usually expressed by the

reflectance $R(\omega)$ and transmittance $T(\omega)$, both of which depend on the frequency of the incident electromagnetic wave. They can be defined as:

$$A(\omega) = 1 - R(\omega) - T(\omega) \tag{1}$$

$$A(\omega) = 1 - |S_{11}|^2 - |S_{21}|^2 \tag{2}$$

Transmittance ($T(\omega) = |S_{21}|^2$ $T(\omega) = |S_{21}|^2$) and reflectance ($R(\omega) = |S_{11}|^2$) are shown separately in the form of S parameters [25].

To describe the characteristics of microwave absorbers, the effective medium parameters, the effective permittivity $\varepsilon_{eff}(\omega)$, and the effective permeability $\mu_{eff}(\omega)$ can be used. Figure 5a,b show the effective permittivity $\varepsilon_{eff}(\omega)$ and the effective permeability $\mu_{eff}(\omega)$, respectively. It can be observed that the real part of both parameters is close to zero at the absorptance frequency, which indicates that the reflectivity is close to zero. Figure 5c shows the simulated effective impedance normalized by the free-space impedance, and the effective impedance of the absorbing structure can be expressed as [26]:

$$Z_{eff} = \sqrt{\frac{\mu_{eff}(\omega)}{\varepsilon_{eff}(\omega)}} = \sqrt{\frac{(1+S_{11})^2 - S_{21}{}^2}{(1-S_{11})^2 - S_{21}{}^2}} \tag{3}$$

The real part of the effective impedance fluctuates around 1 in the 4.5–9.45 GHz frequency range, while the imaginary part is almost zero in the 6.3–8.7 GHz frequency range. We can conclude that the input impedance of the structure is almost matched with the impedance matching free space Z0 of the structure, and the impedance of the microwave absorber is perfectly matched with the free space due to the rational and optimal design of the unit structure. Therefore, the perfect microwave absorptance is achieved by simultaneously reducing transmittance and reflectance to maximize the absorptance rate.

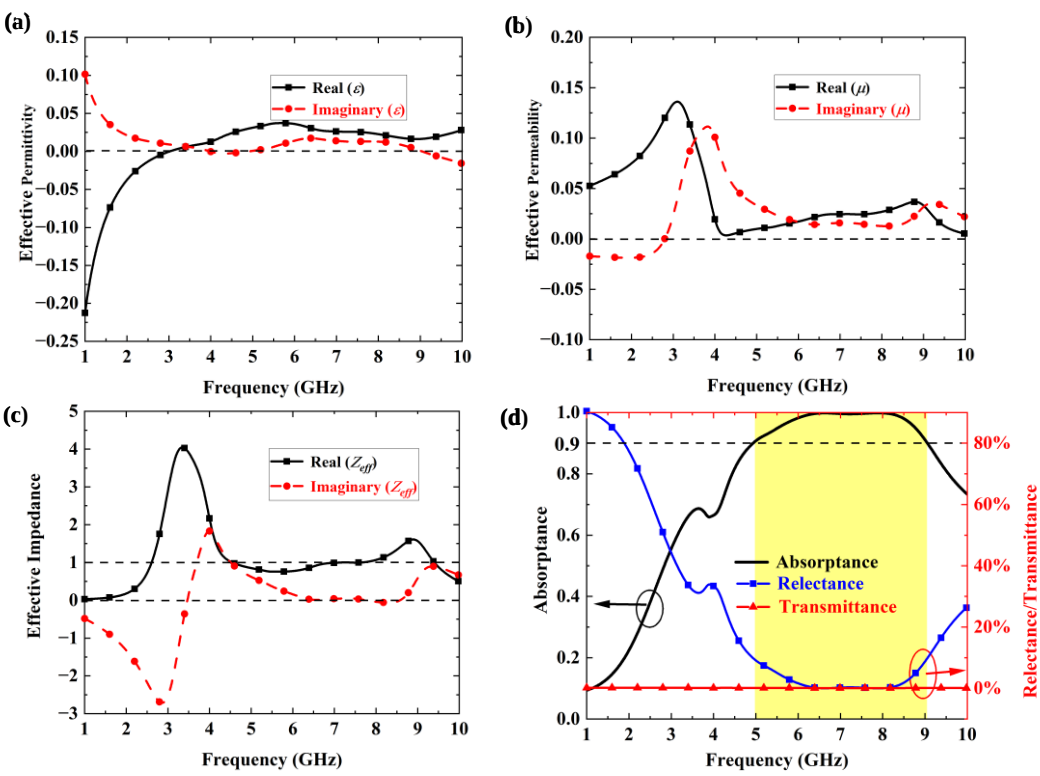

Figure 5. Retrieved constitutive parameters, absorptance, reflectance, and transmittance. (**a**) Effective permittivity. (**b**) Effective permeability. (**c**) Effective impedance. (**d**) Absorptance, reflectance, and transmittance characteristics.

Figure 5d shows the simulated absorptance, reflectance, and transmittance of the proposed absorber. It has a good absorptance characteristic of over 90% in the 5.06–9.01 GHz band.

In order to explain the influence of the upper resistive film on the absorptance performance of the proposed structure, the reflectivity of the absorber at different resistance values (R_{S1}) of the upper layer was investigated. As illustrated in Figure 6, as the resistance of the top layer increases, there is an optimum value of sheet resistance (R_{S1} = 110 Ω/sq) to achieve the lowest reflection coefficient (−45.21 dB). In this case, the absorptance of more than 90% was achieved in the frequency range of 5.06–9.01 GHz.

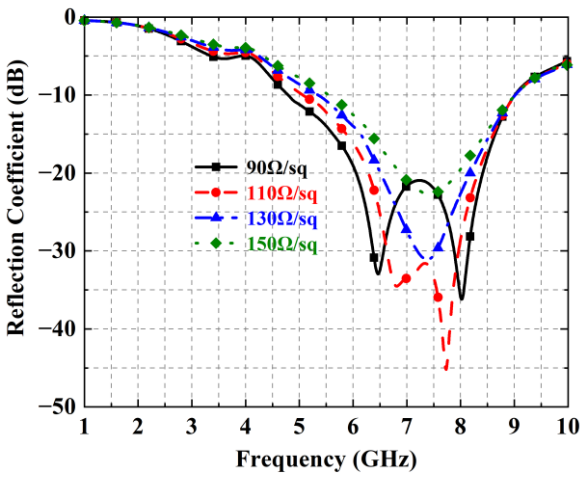

Figure 6. Simulated absorptance of the proposed structure for various upper-layer surface resistance (R_{S1}) values.

To better understand the absorptance mechanism, the surface current distribution on the top layer at 7.72 GHz is shown in Figure 7. The surface current is mainly distributed on the surface of the rectangular unit, as opposed to the circular unit, where a smaller current distribution can be seen. When the current distribution on the surface increases, the ohmic loss on the resistive film also increases, thus converting more electromagnetic energy into heat, thereby the absorptance rate achieves its maximum value.

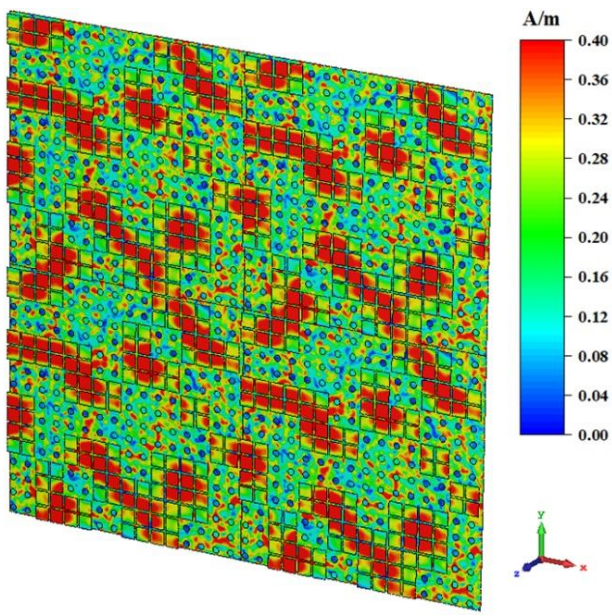

Figure 7. Simulated current distribution at the surface of the absorber structure at 7.72 GHz.

As shown in Figure 8, the absorptance remains above 90% at polarization angles ranging from 0 to 90°, while the absorptance band remains nearly unchanged, which illustrates the polarization insensitivity of the absorber. The simulation confirms the polarization insensitivity of the proposed optically transparent absorber.

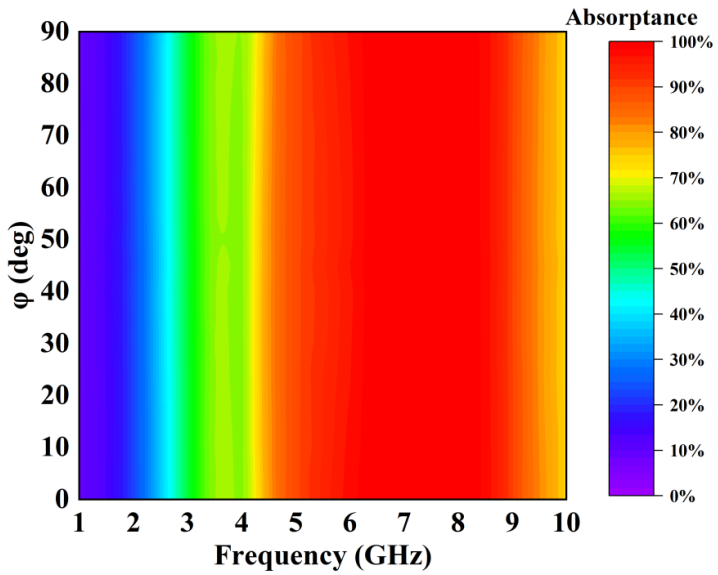

Figure 8. Simulated absorptance of the proposed absorber versus frequency and polarization angle (φ).

In addition to polarization stability, absorbers must have good angular stability in many applications. The simulated absorptance spectra at different oblique illumination incidences for the TE and TM modes show that the absorptance bands slowly and gradually shift to the higher frequency range (Figure 9). When irradiated in the TE mode, the absorptance remains above 90% at incidence angles ranging from 0 to 15°, while the structure of the absorptance band remains almost unchanged. For the TM mode, the stability of the absorptance at different incidence angles is also similar to the TE mode data.

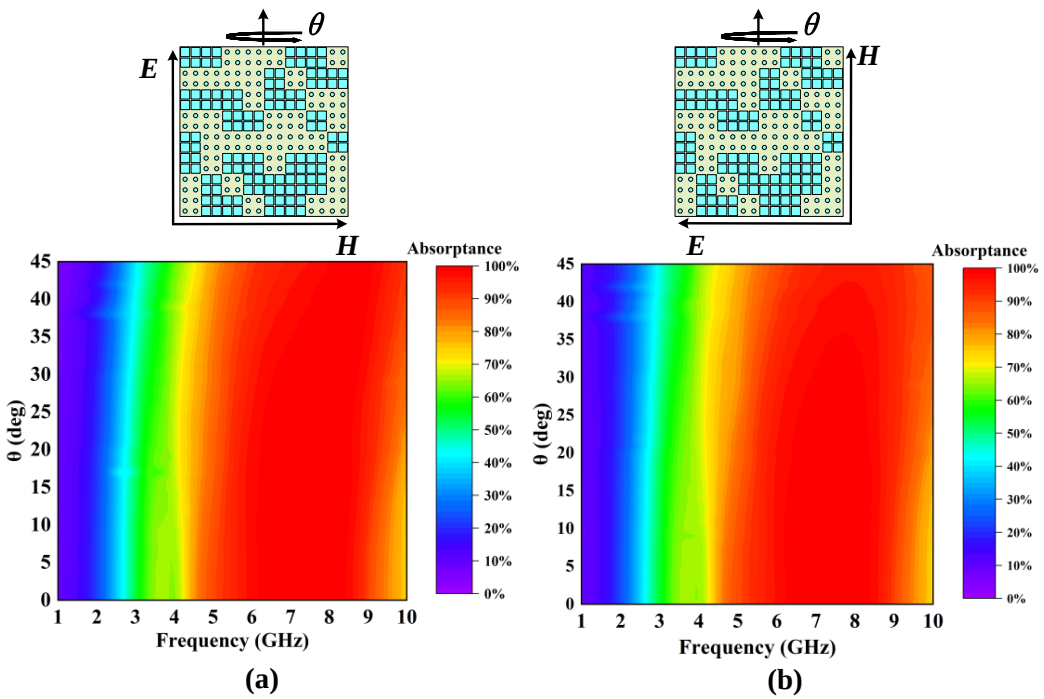

Figure 9. Simulated absorptance as a function of incidence angle θ for: (**a**) TE, and (**b**) TM polarization.

In general, the absorptance of the metamaterial absorber exceeds 80% for incident angles ranging from 0 to 45° over the entire operating bandwidth of both TM and TE modes. This result shows that the proposed design has a reasonably stable angular performance.

The RCS of an ITO-coding metasurface with a cross-section of 240 mm × 240 mm and the perfect electric conductor (PEC) of the same size are simulated and the results are shown in Figure 10. It can be seen that the proposed coding metasurface absorber scatters and spreads the incident electromagnetic wave energy in all directions when the frequency of the incident electromagnetic wave is 7.0 GHz. Furthermore, the energy scattered out in each direction is not strong, indicating that the absorber has good RCS scaling characteristics.

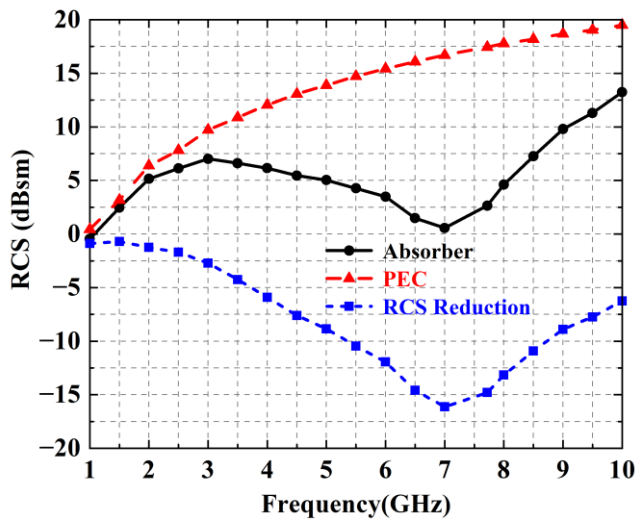

Figure 10. Monostatic RCS magnitude for the main lobe of the proposed absorber versus frequency for horizontally polarized normally incident waves.

At the same time, the absorber achieves an RCS reduction of more than −10 dBsm in the frequency band of 5.3–8.7 GHz, which is significantly higher than the perfect electric conductor (PEC) of the same size.

3. Experimental Verification

In order to verify the absorptance properties of the proposed optically transparent absorber, samples were fabricated and measured in a microwave darkroom. The total size of the sample was 240 mm × 240 mm. The upper ITO film with a thin layer of resistance of 110 Ω/sq was deposited on the PET substrate by magnetron sputtering, and the bottom 8 Ω/sq ITO film was fabricated in the same way. Then, the upper resistive film was patterned by laser ablation of the ITO coating. In order to improve the optical transparency at the same time, a PMMA structure was used in our construction, which also helps to widen the application field. Finally, the upper PET layer and the lower PET layer were adhered to a 5.6 mm PMMA layer, respectively, using transparent double-sided adhesive. The sample optical transparency of the absorber is shown and experiment in Figure 11.

It can be seen in Figure 11a that the prepared experimental samples have good optically transparent properties. Figure 11b depicts the experimental arrangement used for measuring the proposed optically transparent absorber. Figure 11c shows the test environment of the sample. One of the corner antennas acts as the source (transmitting antenna) and the other acts as the end (receiving antenna), where both antennas are connected to a vector network analyzer (VNA).

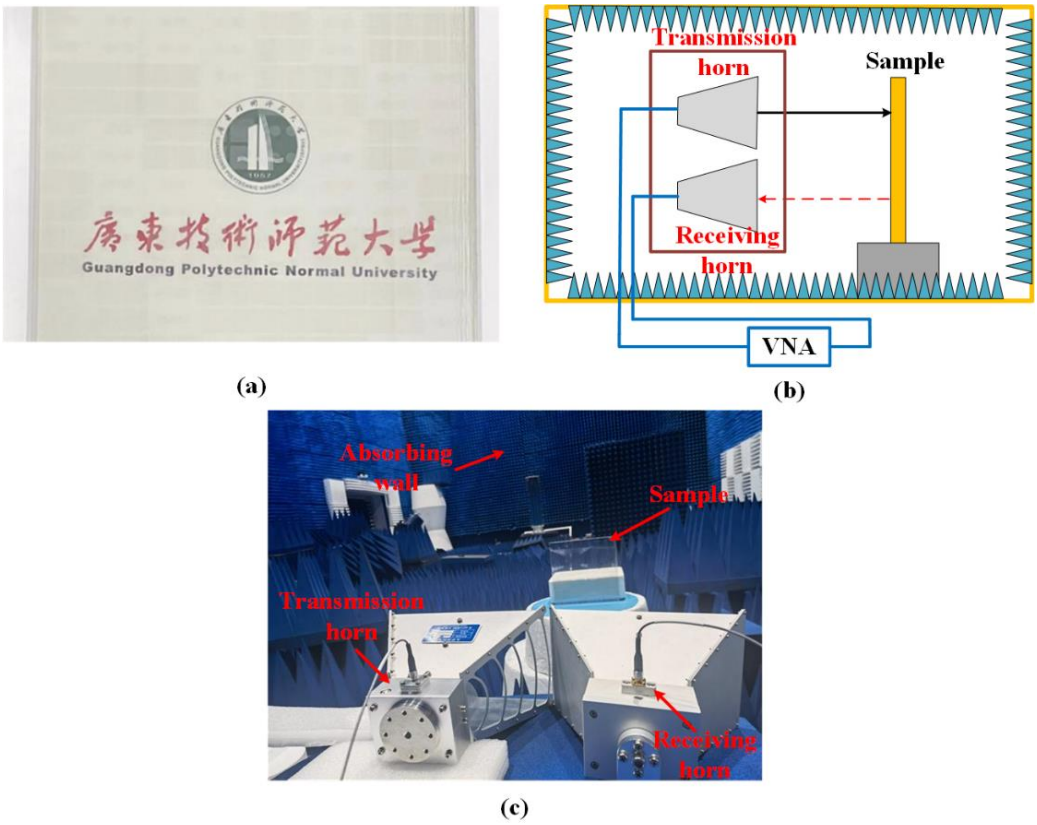

Figure 11. (**a**) Optical transparency experimental sample. (**b**) Schematic of the arrangement used for measuring the proposed optically transparent absorber. (**c**) Photograph of the test environment.

The transmittance (S_{21}) and reflectance (S_{11}) were measured under two different conditions: a metal plate, and the designed absorber. Then, the absorptance is calculated using the following equation [26]:

$$A(\omega) = 1 - (|S_{11}|^2_{sample} - |S_{11}|^2_{metal}) - (|S_{21}|^2_{sample} - |S_{21}|^2_{Air}) \quad (4)$$

The environmental effects can be subtracted using this method, and accurate measurements can be obtained. The experimentally obtained absorptance curve of the sample and S_{11} are shown in Figure 12. To improve the measurement accuracy, the main flap of the antenna should point to the center of the absorber during each measurement.

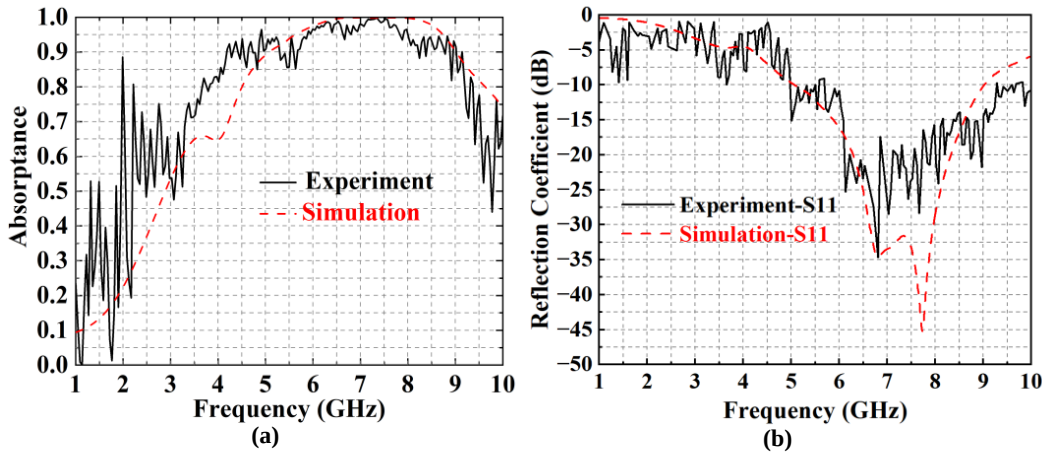

Figure 12. (**a**) The variation of absorptance of the experimental sample. (**b**) Reflection coefficient of the experimental sample as a function of frequency.

4. Discussion

Finally, the characteristics of optically transparent or flexible microwave absorbers reported in recent years are summarized in Figure 13. In comparison to previously reported optically transparent microwave absorbers, the proposed receivers have higher reflection coefficients and better flexible and optically transparent properties.

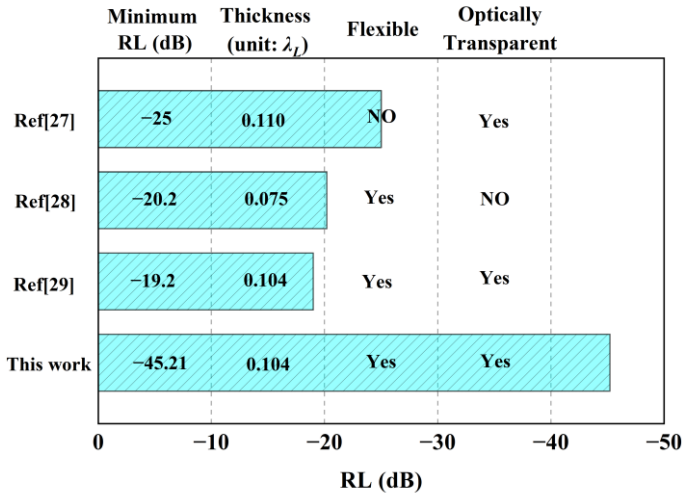

Figure 13. The comparison of the characteristics of previously reported and proposed optically transparent microwave absorbers [27–29].

5. Conclusions

In this paper, a metamaterial absorber with a checkerboard patterned ITO film as the surface is obtained by using flexible and optically transparent wave-absorbing material (ITO-PET) and a coding arrangement of two basic coding units based on the APS-PSO algorithm. The experimental results, which are consistent with the simulation results, show that the absorber has superior performance: over 90% absorptance in the 5.06–9.01 GHz band, high transmittance, and a −10 dBsm RCS reduction in the 5.3–8.7 GHz band. This design also has polarization insensitivity and angular stability, with promising applications in flat panel displays, low radiation glass, special functional window coatings, etc.

Author Contributions: Conceptualization, S.L., G.L. and Y.G. conceived and designed the experiments; Y.G. made the samples, S.L., G.L. and Y.G. performed the experiments; S.L., G.L., Y.G. and Y.L. analyzed the data; S.L. technical construction for coatings; S.L., and G.L. wrote the paper. All authors critically reviewed the content and approved final version for publication. All authors have read and agreed to the published version of the manuscript.

Funding: This work was supported in part by the Yong Innovative Talents Project, Guangdong Province (2019KQNCX069), in part by Special Fund for Science and Technology Innovation Strategy of Guangdong Province (Climbing plan, pdjg2020b0344), and in part by Basic and Applied research of Guangzhou Basic Research Plan (202102020307), and in part by the open funding of Guangdong Provincial Key Laboratory of Millimeter-Wave and Terahertz under Grant 2019B030301002KF2105.

Institutional Review Board Statement: Not applicable.

Informed Consent Statement: Not applicable.

Data Availability Statement: Data underlying the results presented in this paper are not publicly available at this time but may be obtained from the corresponding author upon reasonable request.

Acknowledgments: We would like to thank Wenhua Gu and Chen Fu from Nanjing University of Science and Technology for their help with the testing of the experiment.

Conflicts of Interest: The authors declare no conflict of interest.

References

1. Tak, J.; Choi, J. A wearable metamaterial microwave absorber. *IEEE Antennas Wirel. Propag. Lett.* **2017**, *16*, 784–787. [CrossRef]
2. Bilal, R.; Baqir, M.; Iftikhar, A.; Ali, M.; Rahim, A.; Akhtar, M.N.; Mughal, M.; Naqvi, S. A Novel Omega Shaped Microwave Absorber with Wideband Negative Refractive Index for C-Band Applications. *Optik* **2021**, *242*, 167278. [CrossRef]
3. Mishra, R.K.; Gupta, R.D.; Datar, S. Metamaterial Microwave Absorber (MMA) for Electromagnetic Interference (EMI) Shielding in X-Band. *Plasmonics* **2021**, *16*, 2061–2071. [CrossRef]
4. Badri, S.H.; Gilarlue, M.M.; SaeidNahaei, S.; Kim, J.S. Narrowband-to-broadband switchable and polarization-insensitive terahertz metasurface absorber enabled by phase-change material. *J. Opt.* **2022**, *24*, 025101. [CrossRef]
5. Badri, S.H.; Soofi, H.; SaeidNahaei, S. Thermally reconfigurable extraordinary terahertz transmission using vanadium dioxide. *JOSA B* **2022**, *39*, 1614–1621. [CrossRef]
6. Zhang, C.; Yin, S.; Long, C.; Dong, B.W.; He, D.; Cheng, Q. Hybrid metamaterial absorber for ultra-low and dual-broadband absorption. *Opt. Express* **2021**, *29*, 14078–14086. [CrossRef] [PubMed]
7. Vafapour, Z.; Ghahraloud, H.; Keshavarz, A.; Islam, S.; Rashidi, A.; Dutta, M.; Stroscio, M.A. The potential of refractive index nanobiosensing using a multi-band optically tuned perfect light metamaterial absorber. *IEEE Sens. J.* **2021**, *21*, 13786–13793. [CrossRef]
8. Zhang, M.; Song, Z. Switchable terahertz metamaterial absorber with broadband absorption and multiband absorption. *Opt. Express* **2021**, *29*, 21551–21561. [CrossRef] [PubMed]
9. Victor, V.; Leonid, B.; Valery, S.; Christian, H. Negative refractive index materials. *J. Comput. Theor. Nanosci.* **2006**, *3*, 189–218.
10. Smith, D.R.; Pendry, J.B.; Wiltshire, M.C.K. Metamaterials and Negative Refractive Index. *Science* **2004**, *305*, 788–792. [CrossRef] [PubMed]
11. Zhang, Y.; Lin, P.; Lin, Y. Tunable split-disk metamaterial absorber for sensing application. *Nanomaterials* **2021**, *11*, 598. [CrossRef]
12. Dănilă, O. Spectroscopic assessment of a simple hybrid si-Au cell metasurface-based sensor in the mid-infrared domain. *J. Quant. Spectrosc. Radiat. Transf.* **2020**, *254*, 107209. [CrossRef]
13. Wang, J.; Lang, T.; Hong, Z.; Xiao, M.; Yu, J. Design and fabrication of a triple-band terahertz metamaterial absorber. *Nanomaterials* **2021**, *11*, 1110. [CrossRef] [PubMed]
14. Feng, H.; Xu, Z.; Li, K.; Wang, M.; Xie, W.; Luo, Q.; Chen, B.; Kong, W.; Yun, M. Tunable polarization-independent and angle-insensitive broadband terahertz absorber with graphene metamaterials. *Opt. Express* **2021**, *29*, 7158–7167. [CrossRef] [PubMed]
15. Dănilă, O. Polyvinylidene fluoride-based metasurface for high-quality active switching and spectrum shaping in the terahertz g-band. *Polymers* **2021**, *13*, 1860. [CrossRef] [PubMed]
16. Erkmen, F.; Ramahi, O.M. A scalable, dual-polarized absorber surface for electromagnetic energy harvesting and wireless power transfer. *IEEE Trans. Microw. Theory Tech.* **2021**, *69*, 4021–4028. [CrossRef]
17. Yuan, X.; Chen, M.; Yao, Y.; Guo, X.; Huang, Y.; Peng, Z.; Xu, B.; Lv, B.; Tao, R.; Duan, S.; et al. Recent progress in the design and fabrication of multifunctional structures based on metamaterials. *Curr. Opin. Solid State Mater. Sci.* **2021**, *25*, 100883. [CrossRef]
18. Guillen, C.; Montero, J.; Herrero, J. ITO/ATO bilayer transparent electrodes with enhanced light scattering, thermal stability and electrical conductance. *Appl. Surf. Sci.* **2016**, *384*, 45–50. [CrossRef]
19. Liu, H.; Wang, P.; Wu, J.; Yan, X.; Zhang, Y.; Zhang, X. Analysis of terahertz wave on increasing radar cross section of 3D conductive model. *Electronics* **2021**, *10*, 74. [CrossRef]
20. Landy, N.I.; Sajuyigbe, S.; Mock, J.J.; Smith, D.R.; Padilla, W.J. Perfect metamaterial absorber. *Phys. Rev. Lett.* **2008**, *100*, 207402. [CrossRef]
21. Cui, T.; Qi, M.; Wan, X.; Zhao, J.; Cheng, Q. Coding Metamaterials, Digital Metamaterials and Programming Metamaterials. *Light Sci. Appl.* **2014**, *3*, e218.
22. Liu, B.; He, Y.; Wong, S.; Li, Y. Experimental demonstration of a time-domain digital-coding metasurface for a Doppler cloak. *Opt. Express* **2021**, *29*, 740–750. [CrossRef] [PubMed]
23. Wu, Y.; Wang, J.; Lai, S.; Zhu, X.; Gu, W. A transparent and flexible microwave absorber covering the whole WiFi waveband. *AIP Adv.* **2019**, *9*, 025309. [CrossRef]
24. Im, H.R.; Noh, Y.H.; Hong, I.P.; Kwon, S.H.; Yoon, Y.J.; Hwang, M.J.; Choi, K.S.; Yook, J.G. Monostatic RCS Measurement for Transparent Conducting Oxide Coated Dielectric. *J. Korean Inst. Electromagn. Eng. Sci.* **2019**, *30*, 762–769. [CrossRef]
25. Du, Z.; Liang, J.; Cai, T.; Wang, X.; Zhang, Q.; Deng, T.; Wu, B.; Mao, R.; Wang, D. Ultra-light Plane Meta-absorber with Wideband and Full-polarization Properties. *Opt. Express* **2021**, *29*, 6434–6444. [CrossRef]
26. Hu, X.; Wang, Y.; Wan, Z.; Li, Y.; Li, R.; Li, H.; Cao, Q. Design and analysis of an optically transparent ultra-wideband absorber covering C-, X-, ku-, k-, ka-bands. *Opt. Mater. Express* **2022**, *12*, 1512–1521. [CrossRef]
27. Yang, D.; Yin, Y.; Zhang, Z.; Li, D.; Cao, Y. Wide-angle microwave absorption properties of multilayer metamaterial fabricated by 3D printing. *Mater. Lett.* **2020**, *281*, 128571. [CrossRef]
28. Yao, Z.; Xiao, S.; Jiang, Z.; Yan, L.; Wang, B.-Z. On the design of ultrawideband circuit analog absorber based on quasi-single-layer FSS. *IEEE Antennas Wirel. Propag. Lett.* **2020**, *19*, 591–595. [CrossRef]
29. Xiao, H.; Qu, Z.; Lv, M.; Du, H.; Zhu, W.; Wang, C.; Qin, R. Optically transparent broadband and polarization insensitive microwave metamaterial absorber. *J. Appl. Phys.* **2019**, *126*, 135107. [CrossRef]